Chapter 1

Recent Drifts in pH-Sensitive Reverse Osmosis

Gehan Mohamed Ibrahim and Belal El-Gammal

Additional information is available at the end of the chapter

http://dx.doi.org/10.5772/intechopen.75897

Abstract

Preparation of some smart PAm-ZTS pH-responsive membranes, via reactions between ZTS and PAm under different conditions, was conducted for testing pressure-driven reverse osmosis membranes (PDROMs) in active rejection of Ce^{4+}, Pr^{3+}, Sm^{3+}, Gd^{3+}, Dy^{3+}, and Ho^{3+} ionic lanthanide species in their 3^+ and 4^+ states. Recent theoretical models to designate the membrane operations were mathematically itemized, after selective characterization of the PDROMs. The pH scale response of the membrane was confirmed using static adsorption and hydraulic pervasion result estimations. The flux across the PAm-ZTS membrane decreased with the lowering pH value, with drastic decreases between pH 4 and 7, and was both reversible and durable with pH shifts between ~3 and ~8. At lower pH 3, the individual pores were in a closed-state due to the prolonged structure of the amide chains on the porous surfaces. In contrast, at pH 8, the higher pH value, the membrane pores were in an open-state format, because of the collapsed structures of the amide chains. This grants a clear possible approach for manufacturing some pH-responsive composite membranes and inspires further design for their stimuli-responsive actions by incorporating molecularly designed macromolecules, synthesized by controlled polymerization.

Keywords: pH-responsive membranes, preparation, characterization, morphology, zeta potential, lanthanides, modeling

1. Introduction

Adsorption is the conventional chemical engineering process which is applied in many industries, including oil refineries, petrochemicals, and water and wastewater treatment. Adsorption is an effective separation strategy for the rejection of a wide range of contaminants,

including wastewaters, radioactive waste streams, and separation of radionuclides, but it is not so favorable for the elimination of anions like boron, perchlorates, and nitrates. Adsorption processes would be upgraded by integrating with supplementary processes to obtain hybrid processes with higher removal efficiency [1–5].

Osmosis is a physical technique that has been widely examined by researchers in different branches of science and engineering. Early researchers considered osmosis through naturally occurring materials, and from the mid of the nineteenth century, extraordinary consideration has been given to osmosis through manufactured materials. Following the advance in reverse osmosis over the most recent couple of decades, particularly for forward osmosis applications, the interests in different engineering purposes of osmosis had been impelled. Osmosis, or as it is at present alluded to as forward osmosis, has modern applications in wastewater treatment, sustenance preparing, and seawater/saline water desalination. Other one of a kind of regions of forward osmosis look into incorporate pressure retarding osmosis for era of power from saline and unused water and implantable osmotic pumps for controlled medication discharge [6–8].

2. Different categories of membrane processes

Recently, membrane technology has gained great attention as a powerful separation technique. **Figure 1** shows the main categories of the membrane processes. They are categorized mainly based on the size of the contaminants they can exclude from the input stream. Nanofiltration (NF) is one of the fourth classes of pressure-driven membranes appeared after microfiltration (MF), ultrafiltration (UF), and reverse osmosis (RO). It was first developed in the late 1970s as a variant of reverse osmosis membrane [ROM] with reduced separation efficiency for smaller and fewer charged ions such as sodium and chloride. As the term, NF was not known in the 1970s, such that membrane was initially categorized as either loose/open RO, intermediate RO/UF, or tight UF membrane. The term NF appears to have been first used commercially by the Film-Tec Corporation (now the Dow Chemical Company) in the mid-1980s to describe a new line of membrane products having properties between UF and RO membranes. Owing to the uniqueness and meaningfulness of the word NF, other membrane scientists have begun using it [9–11].

Because of late advancements and advances in osmosis innovation, fascinating film operations, including membrane desalination (MD), pressure retarding osmosis (PRO), and reversed electrodialysis (RED), have developed. These operations are equipped for creating spotless and reasonable power from different waste streams, including brackish water and debilitated water, which generally are viewed as natural liabilities. PRO and RED require blending of a high salinity content (e.g., seawater or brackish water and wastewater, separately) with a low salt content to produce power. MD has demonstrated the possibility to produce freshwater and power as an independent process. Reconciliation of MD with PRO or RED upgrades the execution of these procedures and gives a perfect and practical course to create freshwater and vitality [13–16].

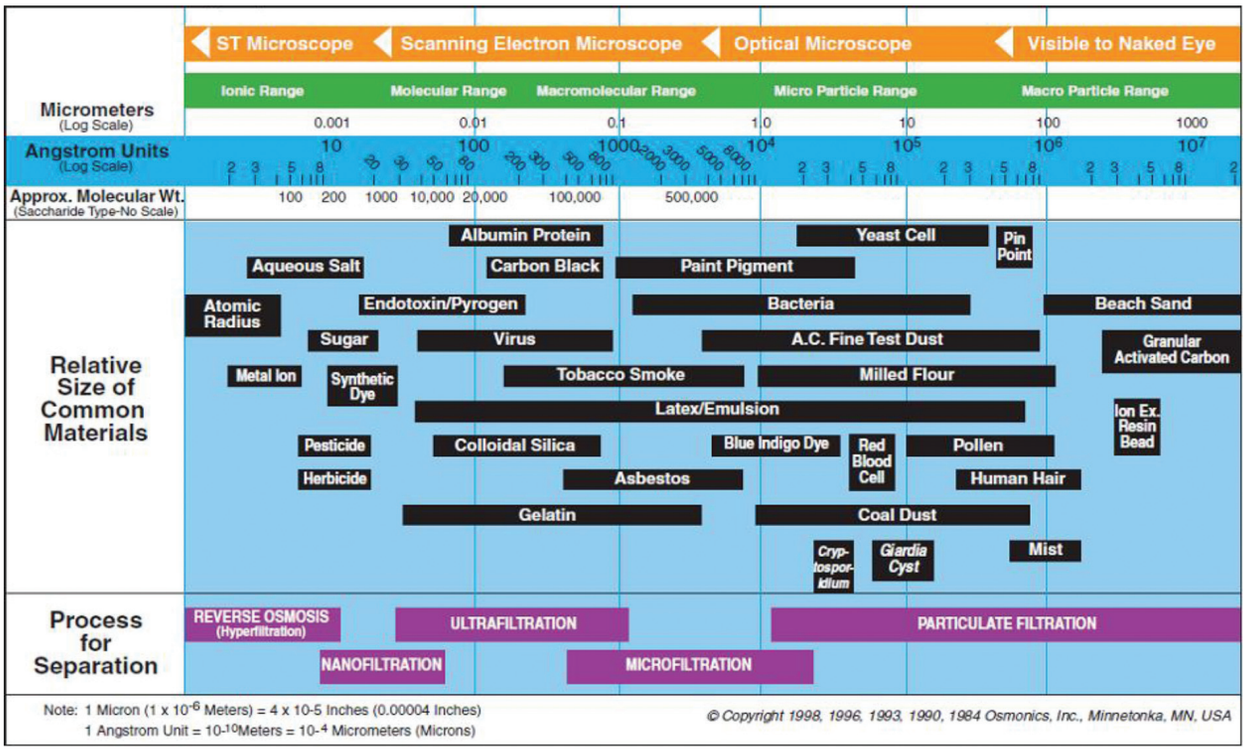

Figure 1. Classification of membrane processes according to separation type, relative size, and approximate molecular weight rejected materials [12].

3. Recent drifts in pH-responsive separation techniques

Recently, membrane technology has gained great attention as a powerful separation technique due to prominent advantages over common processes such as high removal efficiency, low energy consumption, fast kinetic, small footprint, and ease of scale up. They are favored for full-scale applications due to normal operating conditions, high productivity, and low energy consumption. They can efficiently eliminate many contaminants including proteins, macromolecules, natural organic matters (NOMs), dyes, dissolved organic matter (DOM), boron, and compounds responsible for odor and color, from aqueous media. However, the recent achievements for pH-responsive membranes require an ion exchange separation in some cases. **Figure 2** shows a combination between adsorption and membrane separation. The overall removal efficiency of the hybrid process would be enhanced [17–19]. Generally, three different procedures for hybridization of membrane systems with adsorption processes may be found:

- Adsorption treatment before membrane filtration (pretreatment layout)
- Integrated adsorption/membrane processes (IAMPs)
- Adsorption treatment after membrane filtration (post-treatment layout)

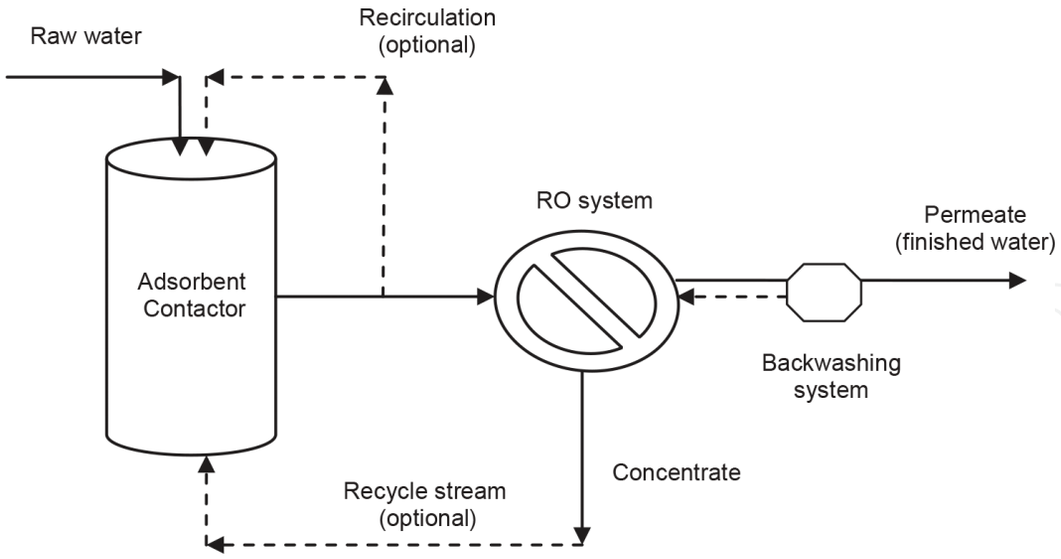

Figure 2. Membrane/adsorption hybrid process with adsorption pretreatment.

The current chapter deals with the adsorption/membrane integrated systems. As could be seen in **Figure 2**, some promising advantages of adsorption/membrane integrated systems could be obtained. They include:

1. Expanding separation efficiency
2. Diminishing process cost
3. Diminished membrane fouling in some cases
4. Straightforwardness of handling and fast control compared to conventional treatments
5. Lower volume of discharge
6. Potential request of beneficial biosorbents
7. Reusability of both membranes and adsorbents
8. Firm removal kinetics
9. Low-energy feed requirements versus adsorption columns, NF and RO systems
10. Low-pressure drop against adsorption columns

4. Fabrication of pH-responsive membranes

Intended for the pre-synthesis of pH-responsive polyacrylamide zirconium titanosilicate (PAm-ZTS) membranes, liquid titanium(IV)chloride (98%), $TiCl_4$, 189.68 [g/mol], 1.728 g/cm^3 (20°C), and zirconium(IV)oxychloride octahydrate powder (>99.5%), $ZrOCl_2.8H_2O$, 321.26752 [g/mol], 1.91 g/cm^3 (20°C), pH value ~1 (50 g/l, H_2O, 20°C), were picked up from Merck Chemicals,

Darmstadt, Germany, while Sigma-Aldrich tetraethyl orthosilicate $(C_2H_5O)_4Si$ 208.33 [g/mol], 0.93 g/cm^3 (20°C), USA was used.

Because of the immense difference between the traditional organic polymers and the corresponding inorganics in their natures and due to strong aggregation of the nanofillers, polymer-inorganic nanocomposite PAm-ZTS membranes cannot be prepared by common schemes such as melt blending and roller mixing. The most frequently secondhand synthesis techniques in the production of nanocomposite membranes can be allocated as three categories [20].

The sol-gel method, the former category secondhand preparation procedure, in which organic monomers, oligomers, or polymers and inorganic nanoparticle precursors are well balanced in solution. The inorganic pioneers were mixed together by gradual addition of tetraethyl orthosilicate, dissolved in equal volumes of bidistilled water and ethyl alcohol with vigorous stirring to zirconium oxychloride octahydrate and titanium tetrachloride solutions, previously dissolved in concentrated hydrochloric acid. The total components are instantly hydrolyzed in an appropriate quantity of water, following to condensation into well-dispersed nanoparticles in the polyacrylamide polymer skeleton with different mole fractions. The reactions' conditions are moderate; usually room temperature, an ordinary atmospheric pressure, and the concentrations of organic and inorganic components are easy to control over the solution. Additionally, the precursor ingredients, as organic and inorganic ingredients could be dispersed in nanometer level in the membranes, and thus the formed membranes are homogeneous. Other techniques as solution mixing and in situ polymerization are used.

5. Characterization of pH-responsive membranes

RO polymerized membranes are different in a couple of characteristics such as material, morphology, transport/separation mechanism, and applications [21–24]. Therefore, a large number of methodologies are required for their characterizations. They can be generally divided into three major tests, that is, methods used for chemical analysis, methods used for physical analysis, and filtration process for assessing membrane separation performance. Depending on the applicable utilization of RO membranes, their stability assessments against chlorination, organic solvent, thermal, and fouling can also be performed to examine their sustainability under specific environments.

Table 1 describes some instrumental methods used in depicting RO membranes with respect to their chemical and physical characteristics, as well as their separation performances and stability. In a wide range, before conducting RO experiments, various techniques can be employed for their characterization in order to obtain a good knowledge of their parameters that are prominent for manufacturing a membrane with the right integration of water flux and solute rejection. For reverse osmosis pH-responsive membranes, zeta potential is well-thought-out as one of the significant parameters to determine the routes and mechanisms that the membranes behave according to its chemical properties.

Property assessment	Instrument/method	Property assessment	Instrument/method
Chemical properties	ATR-FTIR spectroscopy Zeta potential analysis XPS X-ray diffractometry (XRD) Nuclear magnetic resonance (NMR) spectroscopy	Physical properties	SEM/FESEM TEM Atomic force microscopy (AFM) Contact angle analysis PAS
Separation performance	Permeability selectivity	Stability test	Chlorination Solvent Thermal Filtration

Table 1. Assessments on membrane properties and performances based on different analytical instruments/methods.

5.1. Zeta potential

Zeta potential is a surface charge property for RO membranes at different pH environments. The analysis is particularly significant to help recognize the acid–base features of RO membranes and to predict their separation productivity, as well as to consider the fouling propensity of RO at different water pHs [25–27]. Based on the Helmholtz-Smoluchowski equation with the Fairbrother and Mastin approach, zeta potential can be persistent from the measurement of the streaming potential using Eq. (1):

$$\zeta = \frac{\Delta E}{\Delta P} \frac{\mu k}{\varepsilon \varepsilon_{\circ}} \tag{1}$$

where ΔE is the streaming potential, ΔP is the applied pressure, $\boldsymbol{\mu}$ is the solution viscosity, $\boldsymbol{\kappa}$ is the solution conductivity, and ε and $\varepsilon_{\circ}$ are the permittivity of the test solution and free space, respectively. Several assumptions are inherent in this equation. They are (1) flow is laminar, (2) surface conductivity has no effect and has homogeneous properties, (3) width of the flow channel is much larger than the thickness of the electric double layer, and (4) no axial concentration gradient occurs in the flow channel.

The surface zeta potential of ZTS, PAm, and PAm-ZTS, as pH-Responsive membranes, measured at 25°C, are shown in **Figure 3**. Taking a horizontal section at the zero point of charge shows that the isoelectric point of ZTS, PAm, and PAm-ZTS was about 4.01, 5.7, and 7.6, respectively; throughout membrane testing, an electric potential is induced when cations and anions enclosed by the electrical double layer are forced to migrate along with the flow tangential to the ROM surface; in consequence, a potential difference could be initiated. Mostly, the streaming potential of the membrane surface is being measured. The typical pH range applied for determining surface zeta potential of a ROF membrane used to fall within pH 2–12, more preferably, between pH 3 and 9. The pH of the background electrolyte (5 mM KCl, 25°C) can be adjusted by the addition of either an acid, 0.1 M HCl (or HNO_3), or a suitable base electrolyte, 0.1 M NaOH (or KOH) solution. Owing to the workable irreversible change of membrane surface characteristics, it is highly urged to

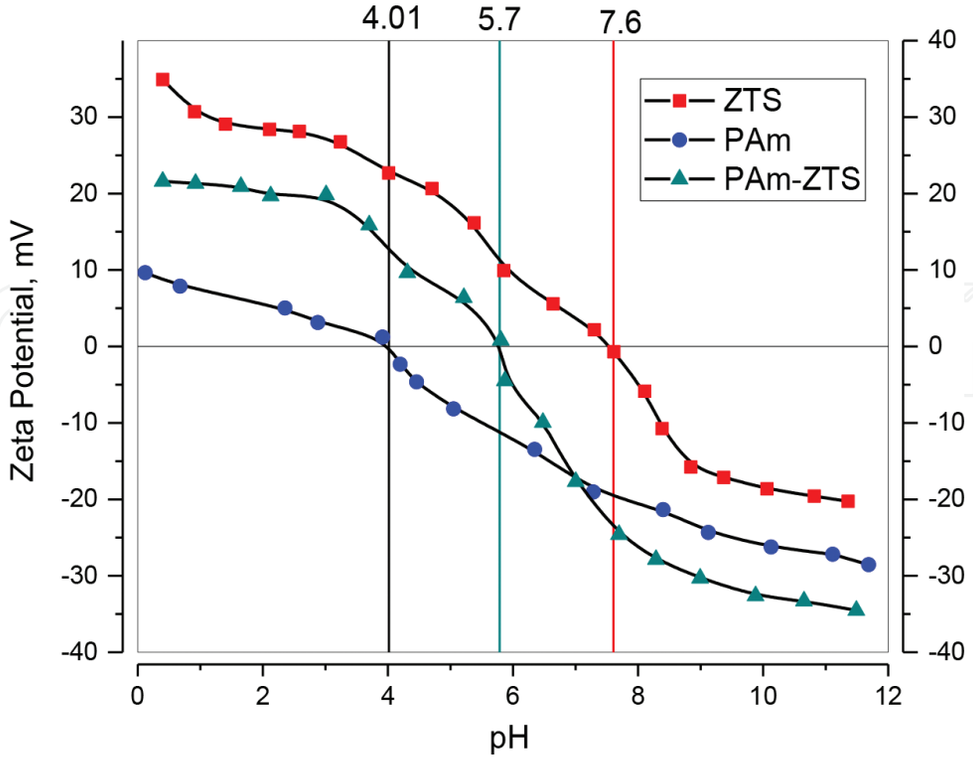

Figure 3. Surface zeta potential as a function of pH for pH-responsive membranes made of ZTS, PAm-ZTS, and Pam, measured at 25°C.

conduct this investigation using two identical freshly prepared ROMs, that is, one for acid titration (pH 6 down to pH 2) followed by another identical membrane for alkali titration (pH 6 up to pH 12).

PAm-ZTS RO membranes tended to have more positive charge owing to the protonation of the amine functional groups. In contrast, the negative charge of RO membranes at higher pHs can be attributed to the loss of functional groups [28–30]. Deprotonation of amine functional groups coupled with either dissociation of the carboxylic acid group or sulfonic acid group on the membrane surface may occur. In brief, in the membranes with organic origin, PAm is more negatively charged than that of that made up of ZTS and PAm-ZTS till pH 7 [25, 31, 32]. Besides showing the positive and negative charge values of a membrane, zeta potential profile can also reveal the isoelectric point (IEP) of the RO membrane at which the membrane surface carries no net electrical charge (i.e., neutral).

Depending on the functional groups of RO surface, a highly positively charged RO membrane could also be prepared, in which this membrane displays a positive zeta potential over a wide range of pH values (pH 2–11). The phenomenon is mainly due to the presence of pendant tertiary amine groups in some polymers used to fabricate the membranes. It was also reported to cause the membrane to be positively charged for pH ranging from 3 to 9 [33, 34]. A summary of the surface zeta potential of some RO membranes made of different monomers at two different pH environments is presented in **Table 2** [25–27].

Type of NF Membrane[a]	IEP (pH)	ζ (mV) at pH 3	ζ (mV) at pH 9
MPF-34 (Koch Membrane Systems)	4.5	~13	~ –34
Desal-5DK (GE Osmonic)	3.9	~18	~ –50
NF 270 (DOW FILMTEC)	3.2	~5	~ –75
BW30 (DOW FILMTEC)	3.6	~2	~ –10
NF90 (DOW FILMTEC)	4.2	~14	~ –24
PIP–TMC–MWCNT NF membrane	2.6	~ –1.2	~ –7
MPD–TMC NF membrane	6.0	~28	~ –11
PIP–TMC–GO NF membrane	5.4	~25	~ –32
PVAm–TMC NF membrane	6.5	~19	~ –12
AEPPS–PIP–TMC NF membrane	4.1	~1.3	~5.6
PES–TA NF membrane[b]	10.7	~32	~6
PIP–*mm*-BTEC NF membrane[b]	–	~28	~4
PEG600–NH_2–TMC NF membrane[b]	~8.9	~19	0

aAEPPS—N-aminoethyl piperazine propane sulfonate, MPD—m-phenylenediamine, *mm*-BTEC—3, 3′, 5, 5′-biphenyl tetraacyl chloride, MWCNT—multi-walled carbon nanotube, GO—graphene oxide, PES–TA—poly (arylene ether sulfone) with pendant tertiary groups, PIP—piperazine, PVAm—polyvinylamine, and TMC—trimesoyl chloride.
bThese NF membranes are positively charged over a wide pH range.

Table 2. Summary of the surface zeta potential of some NF membranes at different pH environments.

It should be noted here that besides surface zeta potential measurement, the conventional titration method can also be employed to evaluate the ion exchange capacity of the RO membrane. Any change in the membrane ion exchange capacity can be related to the amount of charged groups that exist on a membrane.

5.2. Surface topography of PAm-ZTS pH-responsive membranes

In white-LED illumination focused by AFM, as shown in **Figures 4a** and **5a**, the surface topography of the prepared PAm-ZTS was different as the pH of the treatment was switched from three to eight. **Figures 4b** and **5b** explain the three-dimensional image of the pH-responsive membranes. The surface roughness was depicted by the histograms in **Figures 4c** and **5c**, with a broad distribution from less than 50 nm to more than 290 nm, and has a median value of roughly 130 nm in the case of PAm-ZTS treated at pH = 3, while PAm-ZTS treated at pH = 8 has a spread-out distribution between about 20 and 300 nm with an average value of circa 115 nm.

The dissection of **Figures 4a–c** and **5a–c** illuminates the photomicrograph of the cross section in the compact layer morphology of dry/wet phase inversion shear to cast PAm-ZTS asymmetric membrane, in a strained convection dwelling time for 15 s, at pHs 3 and 8, separately. This microstructure had the relatively fit dense skin layer with inconspicuous flaws backed on a highly open nanoporous sublayer containing not only nanovoids but also micro-voids. These

http://dx.doi.org/10.5772/intechopen.75897

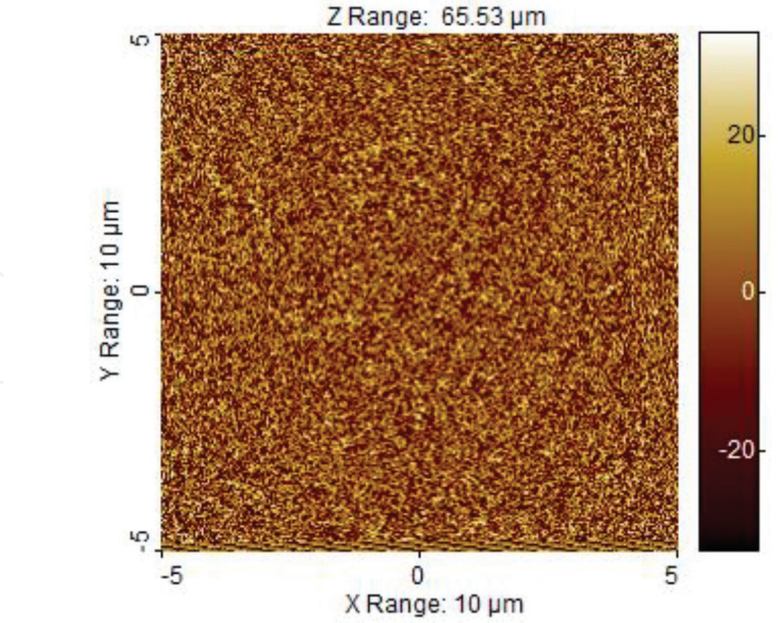

(a)

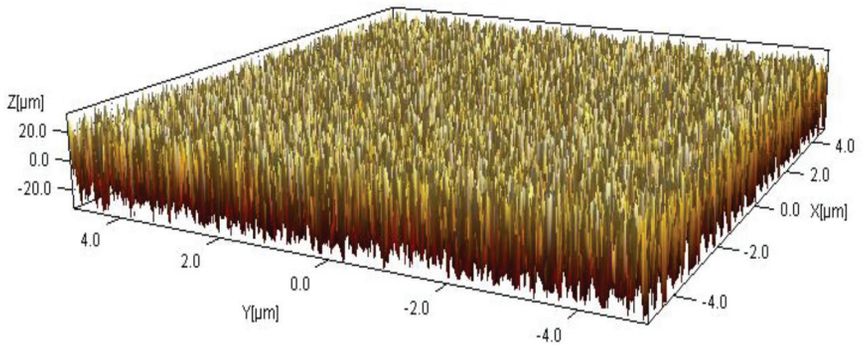

(b)

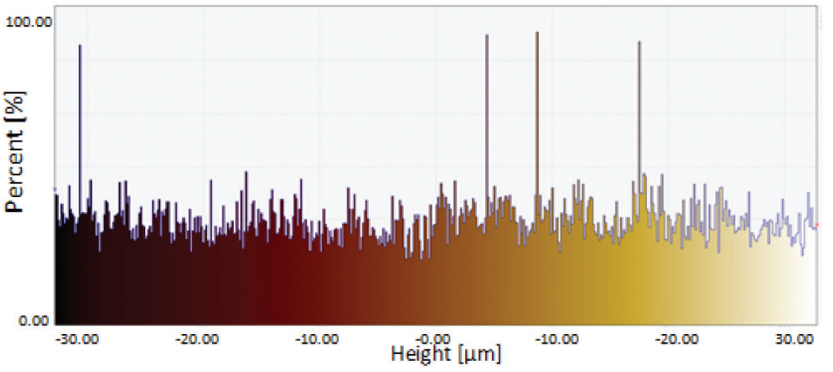

(c)

Figure 4. Surface topography of PAm-ZTS as pH-responsive membrane, measured at 25°C after treatment at pH 3.

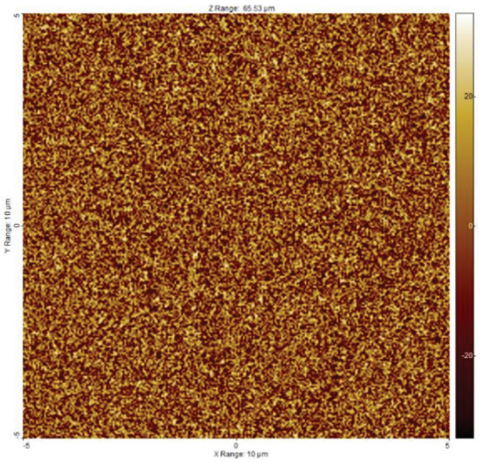

(a)

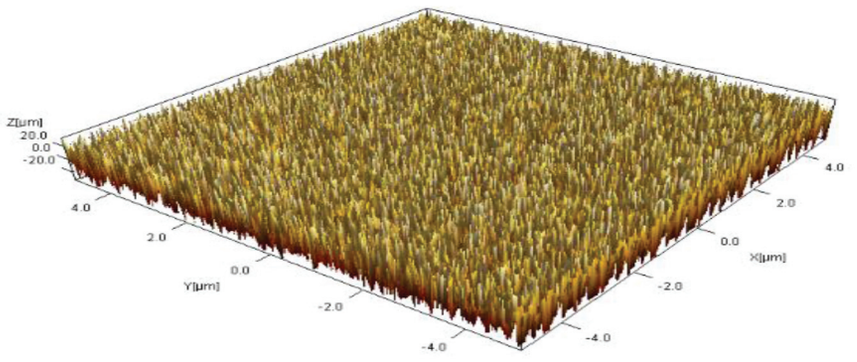

(b)

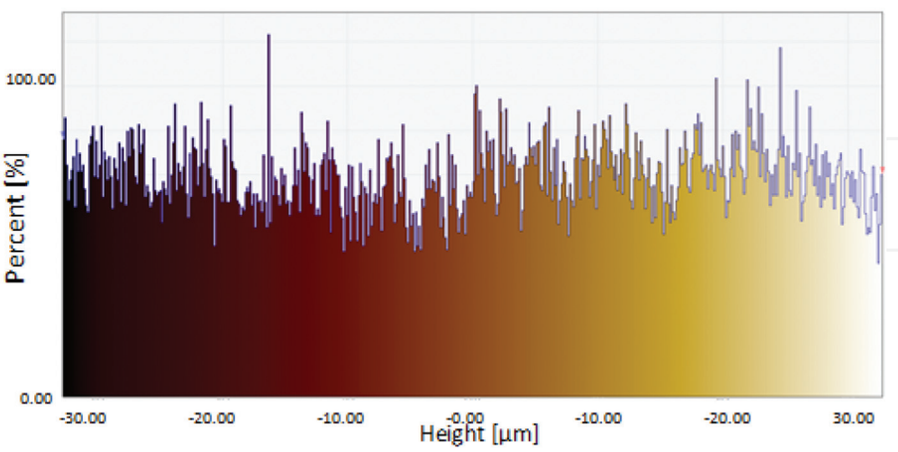

(c)

Figure 5. Surface topography of PAm-ZTS as pH-responsive membrane, measured at 25°C after treatment at pH 8.

were truly similar to those found in the aqueous quenched asymmetric ROMs [35–37]. The nanovoids did not span the width of the ROM evoking that these nanovoids are provoked by disparate mechanisms. In this case, the creation nanopores were formulated by intrusion of non-solvent through defects in the surface layer during wet phase separation, in a step for membrane reinforcement. Additionally, no surface pores could be observed on the outer surface of RO membrane, even at 5000X magnifications 5000X magnifications. This indicated that the diameters of any surface pores were at least less than 20 A°, which would be helpful to be applied for reverse osmosis separation rather than ultrafiltration or nanofiltration.

6. Modeling of pressure-driven membranes

The natural water resources contain solids in two forms, suspended and dissolved [16, 38, 39]. Suspended solid-state matters exist in insoluble particulates, debris, seawater microorganisms, silt, or colloids. Dissolved matters are present as ions, preferably as chloride, sodium, calcium, or magnesium. Principally, all desalination plants incorporate two-key treatment steps, sequentially designed to remove suspended and dissolved matters from their sources.

The first step of pretreatment removes the suspended solids from water resources or the naturally occurring soluble solids that may turn into a solid form and precipitates on the ROMs during separation processes. The second step of the RO system separates the dissolved solids from the pretreated saline source water, thereby producing fresh low-salinity water convenient for human utilization agricultural purposes and industrial implementations.

Subsequent pretreatment is designed for the left solids in the source stream; it includes the dissolved minerals. As long as the desalination system is operated in a manner that prevents these minerals from precipitating on the membrane surface, the ROMs could operate and produce freshwater of persistent nature at a high rate deprived of the need to clean these ROMs for long periods.

Notwithstanding pretreatment systems remove most but not all the insoluble solids contained in the saline source water and may not always effectively protect some of the soluble solids from precipitating on the membrane surface, the suspended solids, silt, and natural organic matter (NOM) that remained which may accumulate on ROM surface causing the loss of membrane productivity. In inclusion, saline water contains microorganisms as well as dissolved organics that could serve as food for these microorganisms. Consequently, a biofilm could form and grow on the ROM surface, causing loss of membrane productivity as well.

The protocol of reduction/loss of productivity of ROMs due to agglomeration of suspended solids and NOM, precipitation of dissolved solids, and/or establishment of biofilm on the ROMs surface is known as membrane fouling (MF). Excessive MF is undesirable since it has a negative impact on ROM productivity; it could also result in an increased consumption of energy for salt separation and in deterioration of product water quality.

6.1. External and internal fouling

The classification of the fouling phenomenon depends on the location of the accumulated rejected salts; it can be viewed as [40, 41]:

1. External or "surface" fouling (EF)
2. Internal fouling (IF)

EF involves accumulation of rejected salts on the surface of the membranes by three distinct paths:

- Construction of mineral deposits (scale)
- Construction of cake of rejected solids, particulates, colloids, and other organic and/or inorganic matters
- Biofilm construction, i.e., growth of colonies of microorganisms on the surface of the membranes, rapidly attachable by excretion of extracellular materials

Typically, the three mechanisms can occur in any combination at any given time. However, external membrane fouling of ROMs is most frequently caused by biofouling.

IF is a regular loss of membrane productivity due to changes in its chemical structure either by physical compaction or by chemical degradation. Physical deterioration of the membrane may result from long-term application of feed stream at pressures higher than that designed for the ROMs; they are designed to handle 83 bars for sea water reverse osmosis membranes and/or by their continued setup at source water temperatures above 45°C, the limit of safe membrane operation. Chemical deterioration results from continuous exposure to strong oxidants, e.g., chlorines, bromines, ozones, permanganates, peroxides chemicals, and very strong acids, typically pH < 3 and alkali at pH > 12.

The difference between EF and IF is somewhat clear; EF could be completely reversed by chemical cleaning, while IF causes permanent damage of the micropores, resulting in an irreversible changes.

6.2. Concentration polarization fouling

Concentration polarization (CP) phenomenon entails the formation of a boundary double layer along the membrane surface, with salt concentration considerably higher than that of the starting injected solution as revealed in **Figure 6** [42–44]. C_b is the salt concentration within the boundary layer; C_s is the salt concentration at the inner membrane surface, and C_p is the lower salt content of the freshwater on the pass through side.

As indicated in **Figure 6**, the flow comes to pass in the boundary layers of the feed/concentrate spacers; two different types are encountered: a convective flow of fresh feed solution from the bulk and diffusion flow of repelled drain salts, coming back into the feed flow. In that concern, the semipermeable ROM is designed to give higher rate of convective flow than the diffusion flow, as the salts and particulate solids discarded tend to pile up with highest salt contents on the inner surface of the ROM. The concentration of solid particulates in the boundary layer

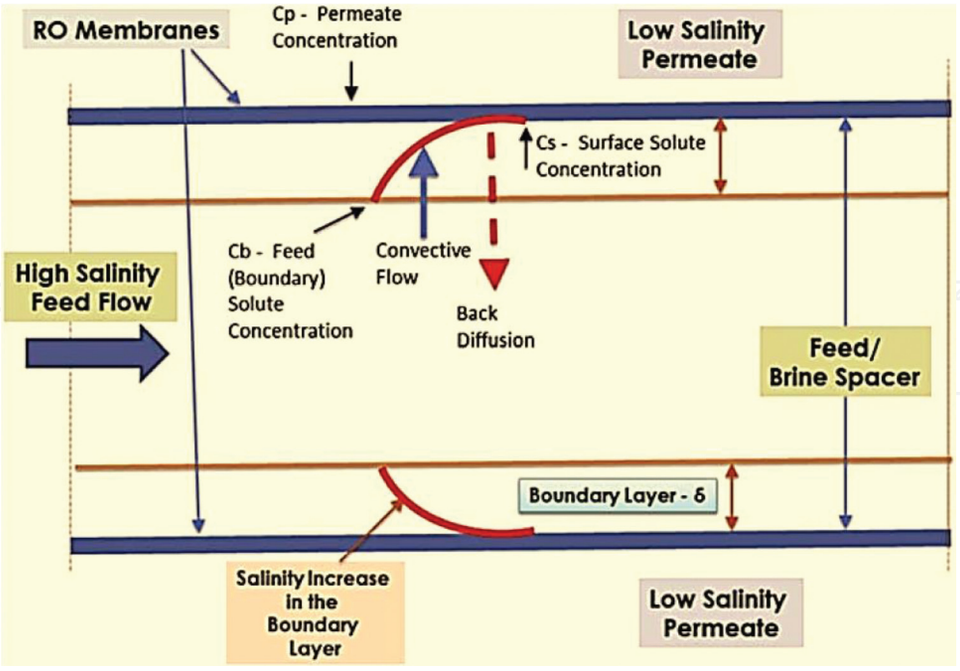

Figure 6. Boundary layers in a membrane-feed spacer. RO, reverse osmosis.

leads to critical negative significances on the ROM function. They include increased osmotic pressure, increased salt extract, creation of hydraulic opposition of water stream, and Induction of scale and fouling on the ROM.

Concentration polarization cannot be evaded; it can only be reduced before taking any corrective measures; concentration polarization should be quantified. This quantification occurs in three separate consecutive paths. They can be emphasized as balancing the chemical and mass balance equations across the boundary layer, balancing the transport equations over the ROM and determination of solute transport equations within the pores of the ROM. System performance can be predicted by simultaneous solution of all these three equations. Based on the type of concentration polarization, there are two classes of models: an osmotic pressure-controlled model and a gel layer-controlling model.

6.3. Osmotic pressure controlled model [OPCM]

In this situation, solute particles form a viscous boundary layer concluded on the surfaces of ROMs [45–47]. Solute concentration increases from the bulk to membrane surface concentration across the mass transfer barrier layer. In this case, the width of the mass transfer boundary layer is constant. At any cross section of the boundary layer for the concentration gradient, $\frac{dc}{dy}$, at the steady state, the solute mass steadiness leads to

$$\left[\left(v_w\, c - v_w\, c_p\right) + D\,\frac{dc}{dy}\right] = 0 \tag{2}$$

where v_w is the permeate flux in $m^3/m^2.s$; c and c_p are the bulk and permeate concentrations in kg/m^3; and D is the solute diffusivity in m^2/s.

Integrating the above equation across the thickness of the mass transfer boundary layer, the governing equation of the flux is obtained as

$$v_w = \left(\frac{D}{\delta}\right)\ln\left(\frac{c_m - c_p}{c\circ - c_p}\right) = k\ln\left(\frac{c_m - c_p}{c\circ - c_p}\right) \tag{3}$$

This equation is well known as the film theory equation. In the above equation, k is the mass transfer coefficient in m/s, δ is the mass transfer boundary layer thickness in m, and c_m, c_p, and c are solute concentrations at the membrane-feed solution interface, in the permeate and in the bulk, generally expressed in kg/m^3, respectively. The mass transfer coefficient is estimated from the following equations depending on the channel geometry and flow regimes. In the rectangular channel, the mass transfer coefficient is estimated using the following Sherwood number relations. For laminar flow (Leveque's equation):

$$Sh = \frac{k\,d_e}{D} = 1.85\left(ReSc\,\frac{d_e}{\mathrm{L}}\right)^{\frac{1}{3}} \tag{4}$$

where, Sh, Re, and Sc are the numbers related to Sherwood, Reynolds, and Schmidt, respectively, d_e is the equivalent diameter in m, and L is the length of the membrane in m. For turbulent flow, Leveque's equation gives rise to (Dittus-Boelter equation):

$$Sh = 0.023(\mathrm{Re})^{0.8}(Sc)^{0.33} \tag{5}$$

In the case of flow through the tube with diameter d in m, the mass transfer coefficient is estimated for laminar flow (Leveque's equation) (Gekas and Hallstrom 1987):

$$Sh = \frac{k\,d}{D} = 1.62\left(ReSc\,\frac{d_e}{\mathrm{L}}\right)^{\frac{1}{3}} \tag{6}$$

In addition, for the turbulent flow, it is calculated from Eq. (5). Now, the transport equation in the flow channel, Eq. (4), must be coupled with the transport law through the porous membrane. It is expressed as Darcy's law:

$$v_w = \mathrm{L}_P\,(\Delta P - \Delta\pi) \tag{7}$$

where $\Delta\pi$ is the osmotic pressure difference between the membrane sides that effectively are related to the quantity of matter, especially the concentration and inversely proportional to the molecular weight of solute; it is a linearly proportional to concentration in the case of a typical salt or lower molecular weight solutes. However, it deviates from linearity in the case of polymers, proteins, and higher molecular weight solutes. In Eq. (2) there are three unknowns, namely, v_w, c_p, and the finally predicted c_m. The comprehensive correlation between the osmotic pressure and concentration, $\pi = ac$, could be pragmatic equation for osmotic pressure difference at the ROM surface as

$$\Delta\pi = \pi_m - \pi_P = a_1[c_m - c_P] + a_2\left[{c_m}^2 - {c_P}^2\right] + a_3\left[{c_m}^3 - {c_P}^3\right] + \ldots\ldots + a_n[c_m n - c_P n] \quad (8)$$

where the constant coefficient is known as the difference between $a_1$and a_{n} and real retention could be defined by c_m and c_P indicated as the coefficients across the ROM phases, respectively, namely, the upstream and downstream phases. Therefore, Eq. (7) can be written in terms of the single parameter c_m using Eq. (2), to reduce the system variables to c_m and v_w, instead of the existing three parameters. The new variables can be attained by solving Eqs. (4) and (6) using an iterative algorithm like the Newton-Raphson equations. This model is known as classic-film model or the osmotic pressure-controlling model.

6.4. Solution diffusion model for RO/NF

The real retention is a partition coefficient, or really the solute flux across the membrane considered using the solution diffusion model described earlier; linear relationship is considered between π and c in the case of salt solution, $\pi = ac$ [42, 43, 48, 49]. In practice, Eq. (6) and the film theory equation, Eq. (4), are only considered. Therefore, the osmotic pressure model could be rewritten as

$$v_w = v_w^o\,[1 - \alpha\,(c_m - c_P)] \quad (9)$$

where

$\alpha = \frac{a}{\Delta p}$ and $v_w^o = L_P\,\Delta P$ are the pure water flux.

The above equation can be equated with the film theory equation and the following equation results:

$$v_w^o\,[1 - \alpha(c_m - c_P)] = k\,\ln\left[\frac{c_m - c_P}{c\circ - c_P}\right] \quad (10)$$

From the solution diffusion model, the solute flux is written as

$$v_w\,c_P = B(c_m - c_P) \quad (11)$$

where B is a constant. Combining Eqs. (8) and (10), the following equation is obtained:

$$v_w^o\,[1 - \alpha(c_m - c_P)] = B\left[\frac{c_m - c_P}{c_P}\right] \quad (12)$$

The above equation can be simplified as.

$$1 - \alpha c_m + \alpha c_P = \beta\left[\frac{c_m - c_P}{c_P}\right] \quad (13)$$

where $\beta = \frac{\mathrm{B}}{\mathrm{v_w^o}}$

From the above equation, the membrane surface concentration is obtained as

$$c_m = c_P\left[1 + \left(\frac{1}{\beta + \alpha c_P}\right)\right] \tag{14}$$

Putting c_m from the above equation into Eq. (9), we get

$$\frac{\beta v_w \circ}{\alpha c_P + \beta} - k \ln\left[\frac{c_P}{(\alpha c_P + \beta)(c \circ - c_P)}\right] = 0 \tag{15}$$

Once more a trial-and-error formula for c_P is tried using a standard iterative technique.

6.5. Kedem-Katchalsky model [KKM]

KKM is considered as another alternate to osmotic pressure one, in which the imperfect retention of the solutes by the RO/NF/UF membranes is incorporated by a reflection coefficient in the equation of the final output flux [50, 51]:

$$v_w = \mathrm{L}_P(\Delta P - \sigma \Delta \pi) \tag{16}$$

where σ is the reflection coefficient. Using π in the above equation gives rise to the following flux equality:

$$v_w = \mathrm{L}_P\left[\Delta P - a\sigma(c_m - c_P)\right] \tag{17}$$

Turning back to the film theory, the concentration on the ROM surface could be rewritten by

$$c_m = c_P + (c^o - c_P)e^{\frac{v_w}{k}} \tag{18}$$

Combining Eqs. (15) and (17), the following equation is obtained:

$$v_w = \mathrm{L}_P\left[\Delta P - a\sigma\left((c^o - c_P)e\frac{v_w}{k}\right)\right] \tag{19}$$

By means of Eq. (19), c_P could be conveyed in terms of $c_m$by using Eq. (10), followed by solving Eq. (18).

6.6. Modified solution diffusion model [MSDM]

The solute transports across the RO/NF/UF membranes are given by adopting both the convective transport and the diffusive transport of the solutes across the voids of the membranes and writing the corresponding flux equation as [52–54]

$$v_w\, c_P = B(c_m - c_P) + (1 - \sigma)v_w\, c_{av} \tag{20}$$

where

$$c_{av} = \frac{c_m - c_P}{\ln\left(\frac{c_m}{c_P}\right)}$$

By combining Eqs. (4) and (19), we get

$$c_P = \frac{\beta}{v_w}\left[\left(c\circ - c_p\right)e^{\frac{v_w}{k}}\right] + \left[\frac{(1-\sigma)\left(c\circ - c_P\right)e^{\frac{v_w}{k}}}{\ln\left(1+\left(\frac{c\circ - c_P}{c_P}\right)e^{\frac{v_w}{k}}\right)}\right] \tag{21}$$

From the mentioned equations between (16) and (21) in c_m, v_w, and c_P, we can iteratively obtain a system prediction.

The MSDM cons are described by the hypotheses that the mass transfer boundary layer is fully developed, whereas the corresponding entrance length required is substantial. Furthermore, physical properties such as diffusivity and viscosity considerably do not vary with concentration, while mass transfer coefficients are calculated from heat-mass transfer analogies applicable for impervious conduits.

On the other hand, the film theory-based osmotic pressure model presents a simple and quick method for quantifying system performance. In order to overcome these cons, the two-dimensional mass transfer boundary layer equation can be solved, and/or detailed pore flow models can be incorporated. Many studies are available including these intricacies of the model.

6.7. Gel layer-controlling model (GLCM)

In this approximation, the gels of concentrated solutes are deposited over the ROM surface with certain thickness in a uniformly fixed distribution of the solutes, and an outer mass transfer boundary film is formed [52, 55]. In that, the film theory, in which the solute concentration extends from feed concentration and gel concentration undergoing drastic variation in viscosity, diffusivity, and density, can be applied to obtain the equation of permeate flux as

$$v_w = k\ln\left(\frac{c_g}{c^o}\right) \tag{22}$$

7. pH-responsive characteristics of PAm-ZTS membrane

The pH-sensitive characteristics of PAm-ZTS membrane were achieved upon static adsorption modes of Ce^{4+}, Pr^{3+}, Sm^{3+}, Gd^{3+}, Dy^{3+}, and Ho^{3+} using both Langmuir and Freundlich Isotherms, as well as the reverse osmosis dynamic mode.

7.1. Langmuir and Freundlich isotherms

The utilization of Langmuir and Freundlich isotherms to depict the complexation process of binding metal ions in the polymer has previously been investigated using the washing and

enrichment methods of the PEUF process [22, 24]. However, the different metal ions were subjected directly to reverse osmosis in the absence of any binding polymers. In this case, the assumption that the concentration of metal ions in the permeates, C_{pi}, symbolizes the concentration of metal that is free in the solution, Y_i, is prepared.

The Langmuir isotherm equation is given by [20, 56, 57]

$$Q = \frac{Q_{max} Y_i}{K_L + Y_i} \tag{23}$$

where: Q is the amount of metal ion, whereas Q_{max} is the maximum capacity of polymer (mg metal/g membrane).

Y_i is the metal free in solution (mg/l).

K_L is the Langmuir equilibrium constant (mg/l).

Langmuir equation gives a linear form:

$$\frac{1}{Q} = \frac{K_L}{Q_{max}} + \frac{1}{Y_i} + \frac{1}{Q_{max}} \tag{24}$$

The Freundlich isotherm equation is given by

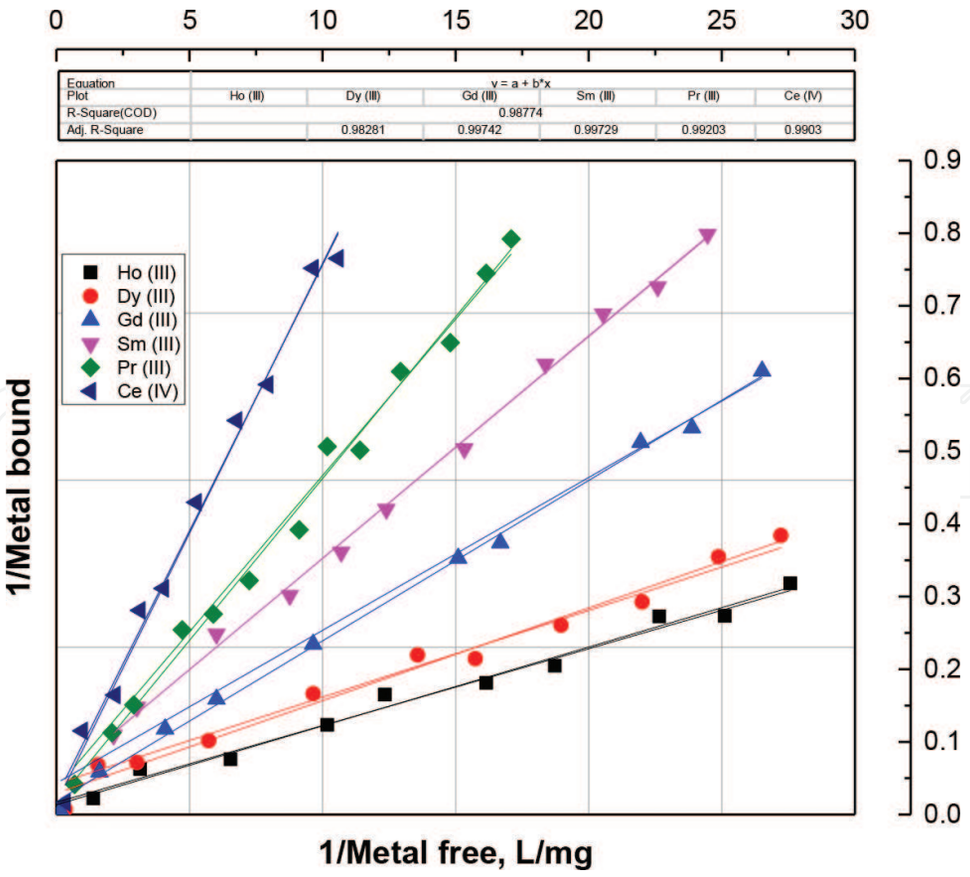

Figure 7. Langmuir isotherm model fits to the experimental data for binding of single metal ions at pH 3.

$$Q = K_F \, Y_i^n \tag{25}$$

where Q is the amount of metal ion, K_F is the Freundlich equilibrium constant ($mg^{1-n} \, g^{-1} l^n$), Y_i is the metal free in solution (mg/l), and n is a constant. Freundlich equation gives a linear form [58–62]:

$$\ln Q = n \ln Y_i + \ln K_F \tag{26}$$

Figure 7 displays the linear regression fits of the Langmuir isotherm to the data obtained for particular metal ions in solution with PAm at pH 3 upon PAm-ZTS surface. The Langmuir isotherm fitted the test data very well (R^2 values >0.98). **Figure 8** exhibits the fits of the experimental data to the Freundlich isotherm at the same pH. Although this model fits the data intelligently well, the fit was not as good as the Langmuir model. This issue discloses that the Langmuir isotherm offers a better description of the binding of metal ions to PAm-ZTS than the Freundlich isotherm [63–66]. However, for all cases, the Q_{max} asset value was found in the following order [20]:

$Ce^{4+} > Pr^{3+} > Sm^{3+} > Gd^{3+} > Dy^{3+} > Ho^{3+}$

These rates can be applicable when considering the retention of the metal ions during the RO process.

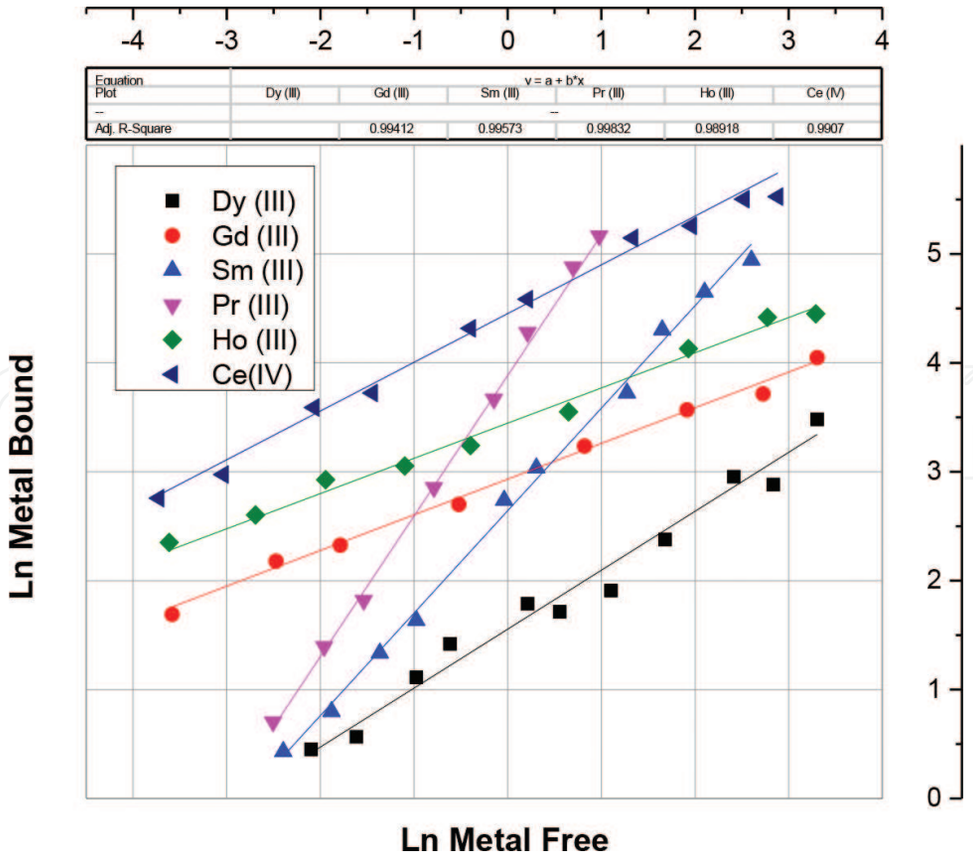

Figure 8. Freundlich isotherm model fits to the experimental data for binding of single metal ions at pH 3.

7.2. Rejection of metal ions

Solute rejections of PAm-ZTS membrane under environmental pH values of 3 and 8 are performed to further evaluate the pH-responsive gating function of membrane. The feed solution is prepared by dissolving Ce^{4+}, Pr^{3+}, Sm^{3+}, Gd^{3+}, Dy^{3+}, and Ho^{3+} in pH buffer with different concentrations mg/l, and the buffers of pH 3 or pH 8 is freshly prepared by adding HCl or NaOH in DI water. The experimental conditions of filtration tests are the same usually used for hydraulic permeability measurements at 0.1 MPa. All the Ce^{4+}, Pr^{3+}, Sm^{3+}, Gd^{3+}, Dy^{3+}, and Ho^{3+} solutions are used as feed solution only within 48 h after preparation. In the filtration test, membranes are conditioned with buffers of pH 3 and pH 8 firstly [67, 68].

Then the permeability of Ce^{4+}, Pr^{3+}, Sm^{3+}, Gd^{3+}, Dy^{3+}, and Ho^{3+} solutions is monitored until the stabilization of membrane is reached and the filtrate is collected. Concentrations of Ce^{4+}, Pr^{3+}, Sm^{3+}, Gd^{3+}, Dy^{3+}, and Ho^{3+} ions in the filtrate solution are measured with Buck Scientific 210 VGP Atomic Absorption Spectrophotometer. The function of examination of the permeate samples for the relevant metal allows the calculation of the observed retention value (R_i) of each metal ion using [9, 42]

$$R_i = \left(1 - \frac{C_{Pi}}{C_{fi}}\right) \times 100 \tag{27}$$

where C_{pi} is the concentration of metal ion, i in the pass through, and C_{fi} is the concentration of metal ion, i in the primary feed solution.

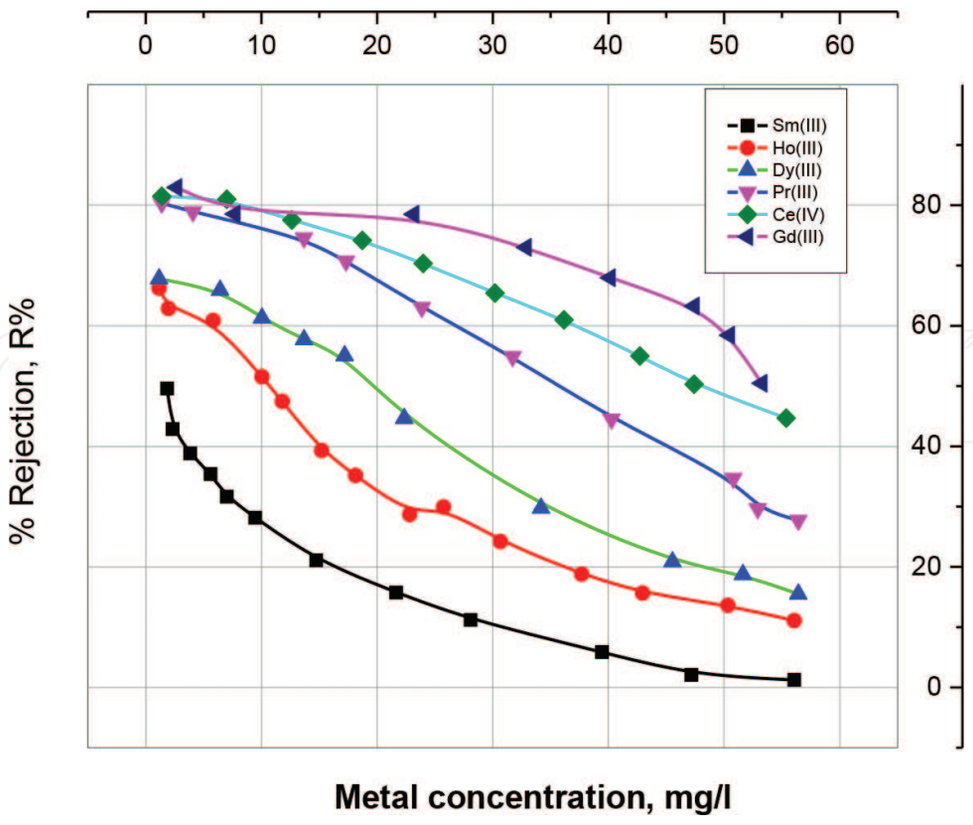

Figure 9. Rejection values of single metal ions at pH 3 for different feed metal concentrations using RO Mode.

Figures 9 and **10** show the rejection coefficient values of single metal ions for different feed metal concentrations using RO Mode at pH ~3 and ~8, respectively. Generally, a high rejection asset value of Ce^{4+}, Pr^{3+}, Sm^{3+}, Gd^{3+}, Dy^{3+}, and Ho^{3+} was observed at low concentrations. Increasing the metal ion content in the feed solution results in a marked decrease in the metal ion rejection, which may be attributed to the closed gates of the membrane. As pH-responsive membrane, PAm-ZTS showed differential rejections according to the pH conditioned. At pH 3, Gd^{3+} and Ce^{4+} were subjected to highest rejection, while Sm^{3+} and Ho^{3+} were rejected with the weakest rates; their rejection coefficients have lowered to less than ten percent at higher concentrations. On the other hand, Pr^{3+} showed the greatest rejection, while Sm^{3+} indicated the quietest rejection. At despicable concentrations, most of the ions are highly rejected at disgusting concentrations that reach about eighty percent. These asset values drop to about thirty to forty percent at higher concentrations. The variation of the rejection as a function of pH in pH-responsive membranes may be explained by the variation of PAm-ZTS conformation because of pH-dependent dissociation of amide hydroxyl. In addition, protonation of amide groups under acidic conditions could be observed [68, 69].

To verify the reversibility and durability of pH-responsive open and closed gating function of the membrane pores, the fluxes of membranes are tested with alternate change of buffer pH between 8 and 3, repeatedly. To characterize the pH-responsive performance, a special coefficient, called pH-responsive coefficient K, is defined as

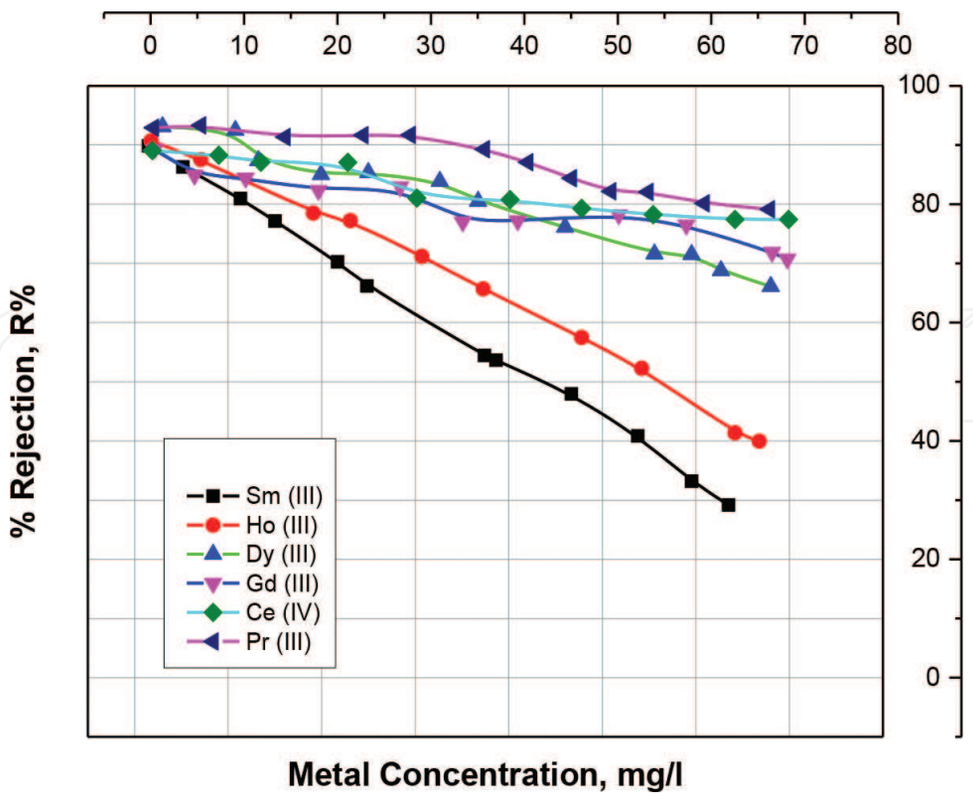

Figure 10. Rejection values of single metal ions at pH 8 for different feed metal concentrations using RO Mode.

$$K = \frac{FLUX_{pH_3}}{FLUXpH_8} \tag{28}$$

where the numerator and denominator represent the transmembrane fluxes at pH 3 and pH 8, respectively. The membrane showed fast response as a function of pH for its potential applications; the fluxes at pH 8 are around 375 l/(m^2 h), while, with changing the feed to pH 3 buffer, the fluxes across the membrane decreased quickly to around 123 l/(m^2 h) within the first recording period, about 40 s. Therefore, the pH-responsive coefficient was about 0.328, indicating a good response of the membrane at the mentioned pHs. This value is mainly a fraction, which contradicts to others found in literature, as other membranes showed a reversed behavior at the same tested pHs [67].

8. Conclusion

A pH-responsive smart PAm-ZTS was prepared by prepared via reactions between zirconium titanosilicate and polyacrylamide under different preparation conditions for testing some lanthanide ions, namely, Ce^{4+}, Pr^{3+}, Sm^{3+}, Gd^{3+}, Dy^{3+}, and Ho^{3+} for their active rejection. The pH response of the membrane was demonstrated using static adsorption and hydraulic permeation results. The water flux of the PAm-ZTS membrane decreased with the decreasing pH value, with the most drastic decrease occurring between pHs 4 and 7, and was both reversible and durable with interchanging pHs between 3 and 8. At pH 3, the membrane pores were in a closed state due to the extended conformation of the amide chains on the pore surfaces. In contrast, at pH 8, the membrane pores were in non-closed state because of the collapsed conformation of the amide chains. The outcomes in this paper afford clear indication to the availability of manufacture and production of pH-responsive composite membranes and can inspire further works on design and preparation of stimuli-responsive membranes through addition of molecularly designed macromolecular additives synthesized by controlled polymerization.

Author details

Gehan Mohamed Ibrahim and Belal El-Gammal*

*Address all correspondence to: belalelgammal@hotmail.com

Faculty of Science, Chemistry Department, University of Bisha, Kingdom of Saudi Arabia

References

[1] El-Naggar IM, Ibrahim GM, El-Gammal B, El-Kady E. Integrated synthesis and characterization of some porous polyacrylamide-based composites for cationic sorption from aqueous liquid wastes. Desalination and Water Treatment. 2014;**52**:6802-6816

[2] El-Gammal B, Ibrahim GM, El-Kholy SH, Shady SA. Ion-exchange equilibrium of cesium/hydrogen ions on zirconium molybdate and zirconium iodomolybdate cation exchangers. Desalination and Water Treatment. 2015;**55**:2121-2143

[3] El-Gammal B, Abdel Hamid M, Ibrahim GM. Ion-exchange properties of ternary CaO-MgO-Al2O3 spinels in pH-controlled aqueous radioactive waste solutions. Desalination and Water Treatment. 2015;**53**:2464-2480

[4] El-Gammal B. Adsorption profiles of some heavy metal ions from aqueous waste solutions using sodium-doped zirconium titanosilicate. Desalination and Water Treatment. 2014;**52**:5952-5964

[5] Khalil T, El-Sweify FH, El-Gammal B, El-Nour FA. Uptake studies of some fission products using ceramic materials. Journal of Radioanalytical and Nuclear Chemistry. 1997;**222**: 61-67

[6] Cheng ZL, Chung TS. Erratum to "mass transport of various membrane configurations in pressure retarded osmosis (PRO)". Journal of Membrane Science. 2017;**539**:358

[7] Chanukya BS, Rastogi NK. Ultrasound assisted forward osmosis concentration of fruit juice and natural colorant. Ultrasonics Sonochemistry. 2017;**34**:426-435

[8] Fischbarg J, Hernandez JA, Rubashkin AA, Iserovich P, Cacace VI, Kusnier CF. Epithelial fluid transport is due to electro-osmosis (80%), plus osmosis (20%). The Journal of Membrane Biology. 2017;**250**:327-333

[9] Khanzada NK, Khan SJ, Davies PA. Performance evaluation of reverse osmosis (RO) pretreatment technologies for in-land brackish water treatment. Desalination. 2017;**406**:44-50

[10] Zaghbani N, Nakajima M, Nabetani H, Hafiane A. Modeling of reverse osmosis flux of aqueous solution containing glucose. Korean Journal of Chemical Engineering. 2017;**34**: 407-412

[11] Shahid MK, Pyo M, Choi YG. Inorganic fouling control in reverse osmosis wastewater reclamation by purging carbon dioxide. Environmental Science and Pollution Research. 2017:1-9

[12] Basile A, Angelo B, Charcosset C. Integrated Membrane Systems and Processes. Newark: Wiley; 2015

[13] Pal P, Chakrabortty S, Nayak J, Senapati S. A flux-enhancing forward osmosis–nanofiltration integrated treatment system for the tannery wastewater reclamation. Environmental Science and Pollution Research. 2017;**24**:15768-15780

[14] Nelson PH. Osmosis and thermodynamics explained by solute blocking. European Biophysics Journal. 2017;**46**:59-64

[15] McCurry DL, Ishida KP, Oelker GL, Mitch WA. Reverse osmosis shifts chloramine speciation causing re-formation of NDMA during potable reuse of wastewater. Environmental Science & Technology. 2017;**51**:8589-8596

[16] Werber JR, Deshmukh A, Elimelech M. Can batch or semi-batch processes save energy in reverse-osmosis desalination? Desalination. 2017;**402**:109-122

[17] Turek M, Mitko K, Piotrowski K, Dydo P, Laskowska E, Jakóbik-Kolon A. Prospects for high water recovery membrane desalination. Desalination. 2017;**401**:180-189

[18] Ali ES, Alsaman AS, Harby K, Askalany AA, Diab MR, Ebrahim Yakoot SM. Recycling brine water of reverse osmosis desalination employing adsorption desalination: A theoretical simulation. Desalination. 2017;**408**:13-24

[19] Touati K, Tadeo F, Elfil H. Osmotic energy recovery from reverse osmosis using two-stage pressure retarded osmosis. Energy. 2017;**132**:213-224

[20] El-Gammal B. Lanthanides diffusion through pH-responsive reverse osmosis membranes. Desalination and Water Treatment. 2014;**52**:4453-4461

[21] Lee J, Choi JY, Choi JS, Chu KH, Yoon Y, Kim S. A statistics-based forward osmosis membrane characterization method without pressurized reverse osmosis experiment. Desalination. 2017;**403**:36-45

[22] Park HM, Jee KY, Lee YT. Preparation and characterization of a thin-film composite reverse osmosis membrane using a polysulfone membrane including metal-organic frameworks. Journal of Membrane Science. 2017;**541**:510-518

[23] Uragami T. Science and Technology of Separation Membranes. Vol. 2. Chichester: John Wiley & Sons; 2017. pp. 274-275

[24] Park SJ, Choi W, Nam SE, Hong S, Lee JS, Lee JH. Fabrication of polyamide thin film composite reverse osmosis membranes via support-free interfacial polymerization. Journal of Membrane Science. 2017;**526**:52-59

[25] Hurwitz G, Guillen GR, Hoek EMV. Probing polyamide membrane surface charge, zeta potential, wettability, and hydrophilicity with contact angle measurements. Journal of Membrane Science. 2010;**349**:349-357

[26] Wilbert MC, Pellegrino J, Zydney A. Bench-scale testing of surfactant-modified reverse osmosis/nanofiltration membranes. Desalination. 1998;**115**:15-32

[27] Elimelech M, Chen WH, Waypa JJ. Measuring the zeta (electrokinetic) potential of reverse osmosis membranes by a streaming potential analyzer. Desalination. 1994;**95**:269-286

[28] Kirby BJ, Hasselbrink EF. Zeta potential of microfluidic substrates: 2 data for polymers. Electrophoresis. 2004;**25**:203-213

[29] Kuo AT, Chang CH, Wei HH. Transient currents in electrolyte displacement by asymmetric electro-osmosis and determination of surface zeta potentials of composite microchannels. Applied Physics Letters. 2008;**92**. DOI: 10.1063/1.2936297

[30] Wang YN, Tang CY. Protein fouling of nanofiltration, reverse osmosis, and ultrafiltration membranes-the role of hydrodynamic conditions, solution chemistry, and membrane properties. Journal of Membrane Science. 2011;**376**:275-282

[31] Salgin S, Salgı U, Soyer N. Streaming potential measurements of Polyethersulfone ultrafiltration membranes to determine salt effects on membrane zeta potential. International Journal of Electrochemical Science. 2013;**8**:4073-4084

[32] Al-Amoudi A, Williams P, Mandale S, Lovitt RW. Cleaning results of new and fouled nanofiltration membrane characterized by zeta potential and permeability. Separation and Purification Technology. 2007;**54**:234-240

[33] Joly L, Ybert C, Trizac E, Bocquet L. Hydrodynamics within the electric double layer on slipping surfaces. Physical Review Letters. 2004;**93**. DOI: 10.1103/PhysRevLett.93.257805

[34] Bukšek H, Luxbacher T, Petrinić I. Zeta potential determination of polymeric materials using two differently designed measuring cells of an electrokinetic analyzer. Acta Chimica Slovenica. 2010;**57**:700-706

[35] Elimelech M, Zhu X, Childress AE, Hong S. Role of membrane surface morphology in colloidal fouling of cellulose acetate and composite aromatic polyamide reverse osmosis membranes. Journal of Membrane Science. 1997;**127**:101-109

[36] Vrijenhoek EM, Hong S, Elimelech M. Influence of membrane surface properties on initial rate of colloidal fouling of reverse osmosis and nanofiltration membranes. Journal of Membrane Science. 2001;**188**:115-128

[37] Tang CY, Kwon YN, Leckie JO. Probing the nano- and micro-scales of reverse osmosis membranes-a comprehensive characterization of physiochemical properties of uncoated and coated membranes by XPS, TEM, ATR-FTIR, and streaming potential measurements. Journal of Membrane Science. 2007;**287**:146-156

[38] Attarde D, Jain M, Singh PK, Gupta SK. Energy-efficient seawater desalination and wastewater treatment using osmotically driven membrane processes. Desalination. 2017;**413**:86-100

[39] Tedesco M, Hamelers HVM, Biesheuvel PM. Nernst-Planck transport theory for (reverse) electrodialysis: II Effect of water transport through ion-exchange membranes. Journal of Membrane Science. 2017;**531**:172-182

[40] Jiang S, Li Y, Ladewig BP. A review of reverse osmosis membrane fouling and control strategies. Science of the Total Environment. 2017;**595**:567-583

[41] Xie Z, Nagaraja N, Skillman L, Li D, Ho G. Comparison of polysaccharide fouling in forward osmosis and reverse osmosis separations. Desalination. 2017;**402**:174-184

[42] Lv L, Xu J, Shan B, Gao C. Concentration performance and cleaning strategy for controlling membrane fouling during forward osmosis concentration of actual oily wastewater. Journal of Membrane Science. 2017;**523**:15-23

[43] Chun Y, Mulcahy D, Zou L, Kim IS. A short review of membrane fouling in forward osmosis processes. Membranes (Basel). 2017;**7**. DOI: 10.3390/membranes7020030

[44] Laqbaqbi M, Sanmartino J, Khayet M, García-Payo C, Chaouch M. Fouling in membrane distillation, osmotic distillation and osmotic membrane distillation. Applied Sciences. 2017;**7**:334

[45] Schulze KD, Hart SM, Marshall SL, O'Bryan CS, Urueña JM, Pitenis AA, Sawyer WG, Angelini TE. Polymer osmotic pressure in hydrogel contact mechanics. Biotribology. 2017. DOI: 10.1016/j.biotri.2017.03.004

[46] de Jesus Junqueira JR, Corrêa JLG, de Mendonça KS, Resende NS, de Barros Vilas Boas EV. Influence of sodium replacement and vacuum pulse on the osmotic dehydration of eggplant slices. Innovative Food Science & Emerging Technologies. 2017;**41**:10-18

[47] Ge Y, Yu F, Tan Y, Zhang X, Liu Z. Comparative Transcriptome sequence analysis of sporulation-related genes of Aspergillus cristatus in response to low and high Osmolarity. Current Microbiology. 2017;**74**:806-814

[48] Zhang M, She Q, Yan X, Tang CY. Effect of reverse solute diffusion on scaling in forward osmosis: A new control strategy by tailoring draw solution chemistry. Desalination. 2017; **401**:230-237

[49] Al-Obaidi MA, Kara-Zaitri C, Mujtaba IM. Scope and limitations of the irreversible thermodynamics and the solution diffusion models for the separation of binary and multicomponent systems in reverse osmosis process. Computers and Chemical Engineering. 2017;**100**:48-79

[50] Merlet RB, Tanardi CR, Vankelecom IFJ, Nijmeijer A, Winnubst L. Interpreting rejection in SRNF across grafted ceramic membranes through the Spiegler-Kedem model. Journal of Membrane Science. 2017;**525**:359-367

[51] Boussouga YA, Lhassani A. Study of mass transfer mechanisms for reverse osmosis and nanofiltration membranes intended for desalination. Journal of Materials and Environmental Science. 2017;**8**:1128-1138

[52] Guo C, Zhou L, Lv J. Effects of expandable graphite and modified ammonium polyphosphate on the flame-retardant and mechanical properties of wood flour-polypropylene composites. Polymers and Polymer Composites. 2013;**21**:449-456

[53] Guha R, Xiong B, Geitner M, Moore T, Wood TK, Velegol D, Kumar M. Reactive micromixing eliminates fouling and concentration polarization in reverse osmosis membranes. Journal of Membrane Science. 2017;**542**:8-17

[54] Xu W, Chen Q, Ge Q. Recent advances in forward osmosis (FO) membrane: Chemical modifications on membranes for FO processes. Desalination. 2017;**419**:101-116

[55] Lin Y-L. Effects of organic, biological and colloidal fouling on the removal of pharmaceuticals and personal care products by nanofiltration and reverse osmosis membranes. Journal of Membrane Science. 2017;**542**. DOI: 10.1016/j.memsci.2017.08.023

[56] El-Kamash AM, El-Gammal B, El-Sayed AA. Preparation and evaluation of cerium(IV) tungstate powder as inorganic exchanger in sorption of cobalt and europium ions from aqueous solutions. Journal of Hazardous Materials. 2007;**141**:719-728

[57] Ibrahim GM, Ahmad MI, El-Gammal B, El-Naggar IM. Selectivity sequence of multivalent lanthanides for their separation on Antimonate based exchangers. Separation Science and Technology. 2011;**46**:2549-2565

[58] Metwally SS, El-Gammal B, Aly HF, Abo-El-Enein SA. Removal and separation of some radionuclides by poly-acrylamide based Ce(IV) phosphate from radioactive waste solutions. Separation Science and Technology. 2011;**46**:1808-1821

[59] Ibrahim GM, El-Gammal B, El-Naggar IM. Synthesis and characterization of novel materials, tin potassium vanadate and zirconium potassium vanadate inorganic multicomponent ion exchangers. Separation Science and Technology. 2011;**46**:664-678

[60] El-Gammal B, Ibrahim GM, El-Nahas HH. Thermodynamic and sorption behavior of U (VI) and Th(IV) on unsaturated polyester - Styrene polymeric beads. Journal of Applied Polymer Science. 2006;**100**:4098-4106

[61] El-Gammal B, Metwally SS, Aly HF, Abo-El-Enein SA. Verification of double-shell model for sorption of cesium, cobalt, and europium ions on poly-acrylonitrile-based Ce(IV) phosphate from aqueous solutions. Desalination and Water Treatment. 2012;**46**:124-138

[62] Ibrahim GM, Ahmad MI, El-Gammal B. Structural development of TMMA and SSQXN-8 as porous chelating resins. Journal of Applied Polymer Science. 2009;**113**:3038-3048

[63] El-Gammal B, Shady SA. Chromatographic separation of sodium, cobalt and europium on the particles of zirconium molybdate and zirconium silicate ion exchangers. Colloids and Surfaces A: Physicochemical and Engineering Aspects. 2006;**287**:132-138

[64] Shady SA, El-Gammal B. Diffusion pathways of sodium and cesium ions in the particles of titanium(IV) antimonate. Colloids and Surfaces A: Physicochemical and Engineering Aspects. 2005;**268**:7-11

[65] El-Gammal B, Allan KF. Ion exchange reversibility of some radionuclides on zirconium Tungstosuccinate and zirconium Tungstosalicylate at their solid-liquid interfaces. Separation Science and Technology. 2012;**47**:131-146

[66] El-Nahas HH, Khalil FH, Ibrahim GM, El-Gammal B. Preparation of unsaturated polyester–styrene beads using gamma irradiation and chemical polymerization routes for use in the recovery of some alkali metal ions. Journal of Applied Polymer Science. 2007; **104**:1149-1160

[67] Oh Y, Armstrong DL, Finnerty C, Zheng S, Hu M, Torrents A, Mi B. Understanding the pH-responsive behavior of graphene oxide membrane in removing ions and organic micropollulants. Journal of Membrane Science. 2017;**541**:235-243

[68] Moula Karimdjy M, Tallec G, Fries PH, Imbert D, Mazzanti M, Karimdjy MM, Tallec G, Fries PH, Imbert D, Mazzanti M. Confinement of a tris-aqua Gd(III) complex in silica nanoparticles leads to high stability and high relaxivity and suppresses anion binding. Chemical Communications. 2015;**51**:6836-6838

[69] Ragavan AJ, Adams DV. Nuclear Materials. Hauppauge: Nova Science Publishers; 2011. pp. 1-46

IntechOpen